J Solid State Electrochem (2008) 12:1653–1661
DOI 10.1007/s10008-008-0551-1

ORIGINAL PAPER

AC impedance measurement of cystine adsorption at mild steel/sulfuric acid interface as corrosion inhibitor

Muzaffer Özcan

Received: 12 January 2008 / Accepted: 13 March 2008 / Published online: 12 April 2008

Abstract Alternating current (AC) impedance measurements of mild steel/sulfuric acid interface in the absence and in the presence of various concentrations of cystine (Cys–Cys) have been carried out in the 100 kHz–10 mHz frequency range. The results revealed that Cys–Cys is a good and effective inhibitor for mild steel corrosion in 0.5 M H_2SO_4 and its percent inhibition efficiency changes with its concentration. Changes in impedance parameters indicated the adsorption of Cys–Cys on the mild steel surface, which was verified by scanning electron microscope (SEM) and atomic force microscope (AFM) photographs. Adsorption of Cys–Cys on mild steel surface was found to obey the Langmuir adsorption isotherm with a standard free energy of adsorption $\left(\Delta G^{\circ}_{ads}\right)$ of −33.2 kJ/mol. Energy gaps for the interactions between mild steel surface and Cys–Cys molecule were found to be close to each other showing that Cys–Cys owns capacity to behave as both electron donor and electron acceptor.

Keywords Corrosion · Inhibitor · Adsorption · Cystine · AC impedance · Quantum chemical calculations

Introduction

It is practical to determine the double-layer capacitance to study the adsorption of the organic molecule at the metal/solution interface in corrosion studies [1]. Double layer capacitance can be determined by a variety of methods, but in recent years, AC impedance spectroscopy has widely been preferred [2–14].

It is common to perform the analysis of impedance data with Nyquist complex plane plots or Bode plots over a wide frequency range so as to determine the elements of an equivalent circuit model that represents the metal/solution interface. Relative changes in these elements, such as charge transfer resistance (R_{ct}), double layer capacitance (C_{dl}) etc., can yield valuable mechanistic information for the stages concerning the corrosion degradation of the metal [15].

On the basis of alternating current (AC) impedance theory, experimental curves showing the imaginary component of the impedance as a function of the real component for a range of frequencies (complex plane plots) must form a semicircle whose center lies on the real axis [16]. However, it is often experimentally observed that complex plane plots are depressed semicircles having a center below the real axis.

Seeing that experimentally obtained complex plane plots are depressed semicircles with a center below the real axis, application of the parameters extracted from these complex plane plots to the real systems under practical conditions, as though they were perfect semicircles, is an open question.

The sulfur containing amino acids have been studied as green inhibitors against corrosion of mild steel and of low carbon steel in H_2SO_4 solution [17–20]. Less attention has been paid, however, to the inhibition properties of Cys–Cys [21]. To the best of my knowledge any theoretical calculation has not been applied to Cys–Cys in corrosion studies.

As a consequence, this study has several objectives:

– to carry out AC impedance measurements of mild steel/sulfuric acid interface in the absence and in the presence of various concentrations of Cys–Cys,

M. Özcan (✉)
Department of Science and Technology Education,
Cukurova University,
01330 Adana, Turkey
e-mail: ozcanm@cu.edu.tr

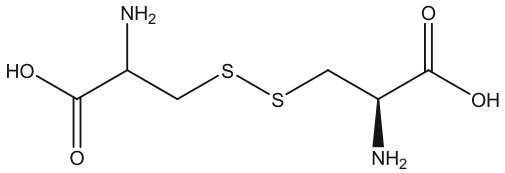

Fig. 1 Molecular structure of Cys–Cys molecule

- to extract kinetic parameters from experimental complex plane plots without and with taking into account the depression,
- to improve the comprehension of the performance of Cys–Cys as corrosion inhibitor by applying quantum chemical calculations

Chemical structure of Cys–Cys is given in Fig. 1.

Experimental

Materials

The working electrode was a cylindrical rod prepared from a mild steel rod having the composition C, 0.11; Mn, 0.45; Si, 0.25; S, 0.050; P, 0.040 and remainder iron. The rod was inserted into a polyester resin, leaving only 0.5 cm^2 of the surface area subjected to the corrosive solution. Before the each experimental run, the working electrode was mechanically polished with a series of emery papers ended with the 1200 grade to a mirror finish, followed by thorough rinsing in acetone and distilled water and dried with soft paper then immediately inserted into the glass cell containing 100 ml of solution. All the experiments were done at 25±1 °C in solutions open to the atmosphere under unstirred conditions after 30 min of exposure time. An Ag/AgCl electrode was used as the reference and a platinum electrode (1 cm^2) was used as the counter electrode. Distilled water and analytical reagent-grade H_2SO_4 (Merck) were used for preparing solutions. The concentrations range of Cys–Cys (Merck) employed were 0.1 to 5 mM. The higher concentrations were increased up to 5 mM since the percent inhibition efficiency is decreased with further increase.

Methods

The experiments were carried out using a conventional three-electrode electrochemical cell. The AC impedance measurements were carried out at corrosion potential using CHI 604A AC electrochemical analyzer with a serial number of 64721A. Twelve points per frequency decade were measured in the frequency range 100 kHz–10 mHz using 5 mV rms sinusoidal perturbation. The impedance parameters were calculated by fitting the experimental complex plane plots to an equivalent circuit using Zview software from Scribner Associates.

Polarization resistance measurements were performed with a scan rate of 1 mVs^{-1} in the range of ±10 mV vs E_{corr}. Polarization curves recorded again with a scan rate of 1 mV s^{-1} in the range of −250mV to +250mV vs E_{corr}, the cathodic potential was chosen as the initial potential.

SEM images were taken using a Carl Ziess Evo 40 SEM instrument at high vacuum and 10 kV EHT, AFM images were taken with Park SYSTEMS using non-contact mode.

In view of the precision and compatibility of the ab initio method, B3LYP [22, 23] hybrid functional of density functional theory (DFT) on the basis set of 6–311**G(d,p) was used to carry out a full geometry optimization of Cys–Cys molecule. All theoretical calculations were carried out using Gaussian 03W program [24]. The frontier molecular orbital surfaces were visualized using Gauss View [25].

Results and discussion

Experimental study

Figure 2 shows AC impedance results of mild steel/sulfuric acid interface obtained in the absence and in the presence of various concentrations of Cys–Cys in the form of complex plane plots.

The complex plane plots in all levels of Cys–Cys concentrations are characterized by one semicircular capac-

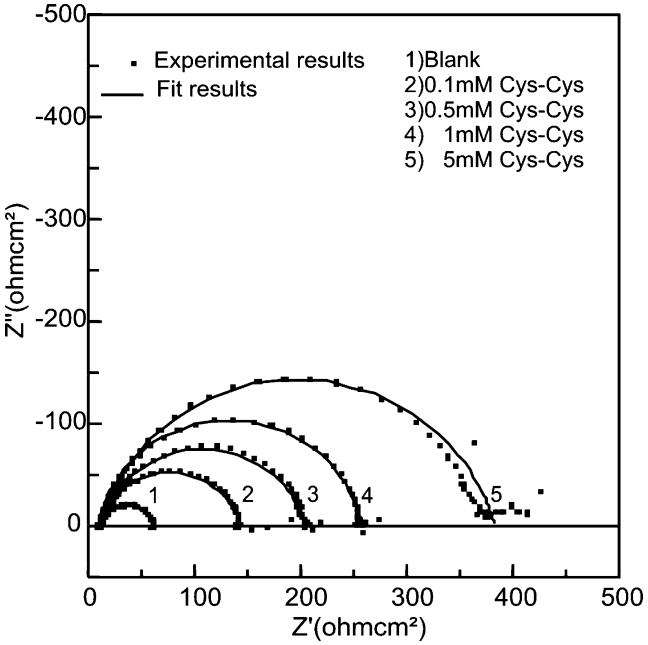

Fig. 2 Complex plane plots for mild steel in 0.5 M H_2SO_4 solution in the absence and in the presence of various concentrations of Cys–Cys

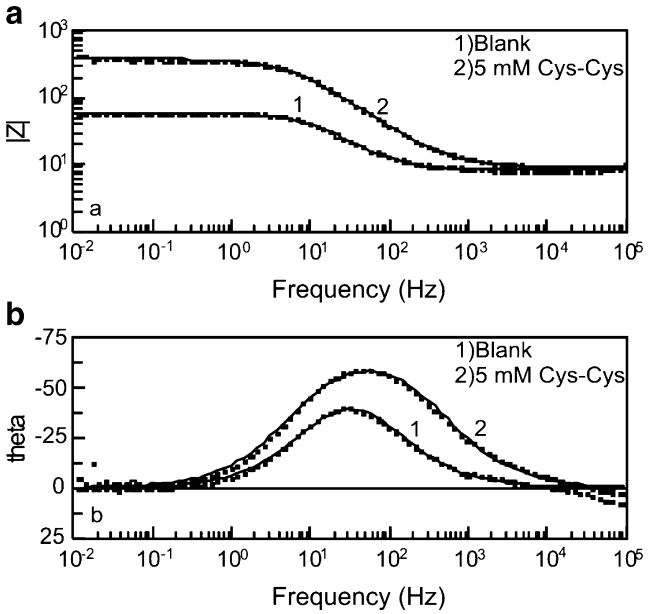

Fig. 3 Bode plots, Z vs frequency (**a**) and θ vs frequency (**b**), for mild steel in 0.5 M H_2SO_4 solution in the absence and in the presence of 5 mM Cys–Cys

itive loop corresponding to one time constant in Bode phase plots (Fig. 3, representative example).

It is apparent that increasing the concentration of Cys–Cys brings about an increase in the diameter of the semicircular capacitive loop (Fig. 2), in the impedance of the double layer (Fig. 3a), and in the maximum phase angle (Fig. 3b).

The general overview of the AC impedance results meets the expectations from the theory of technique, but it must be noted that the capacitive loops are depressed ones with centers under the real axis even though they have a semicircle appearance. Deviations of this kind are mostly referred to as frequency dispersion and they are attributed to irregularities and heterogeneities of the solid surfaces [26]. In addition in the real corrosion systems, the double layer on the interface of metal/solution does not behave as a real capacitor. On the metal side of the double layer, the charge distribution is controlled by electron, whereas on the solution side it is controlled by ions [4]. The high frequency part of the impedance and phase angle reflects the behavior of heterogeneous surface layer, whereas the low frequency part shows the kinetic response for the charge transfer reaction [27].

For the appraisal of the experimental complex plane plots, equivalent circuit models, which physically correctly represent the systems under investigation, must be applied. The simplest model consists of the solution resistance, R_s, in series with the parallel combination of double layer capacitance (C_{dl}) and charge transfer resistance (R_{ct}); in complex plane presentation, this connection of circuit elements yields a perfect semicircle. If this is the case encountered rarely in real corrosion systems, then the double layer capacitance values can be calculated from Nyquist plots and from Bode plots using Eqs.1a and 1b, respectively [28].

$$C_{dl} = \frac{1}{\omega_{max} R_{ct}} \tag{1a}$$

$$C_{dl} = \frac{1}{\omega_{max} R_{ct}} \left(1 + \frac{R_{ct}}{R_s}\right)^{1/2} \tag{1b}$$

The definitions of all the parameters in these equations are commonly found elsewhere in literature [1, 15]. The difference between these two equations is that the frequency at which θ is maximum selected for Bode plot is not the same as the frequency at which Z'' is maximum selected for complex plane plot.

It should be thought that how realistic it is to use C_{dl} values determined using Eqs. 1a and 1b from depressed semicircles as if they were perfect semicircles in the calculation of the quantitative system parameters. Calculations made by using these C_{dl} values will result in high and/or low estimation of the parameters. The C_{dl} values determined from experimental results using the Eqs. 1a and 1b are given in Table 1.

Application of the mentioned circuit in the modeling of the interfaces in this study did not yield a satisfactory fit to the experimental complex plane plots. The deviation of the theoretical impedance from the experimental one shows the inadequacy of the fit (Fig. 4a, representative example for which the fit errors are about 12.5%). This is ascribed to the usage of the ideal circuit elements, e.g., resistor and capacitor, in the equivalent circuit. Replacement of the double layer capacitor (C_{dl}) with the constant phase element (CPE) significantly improved the quality of the fit (Fig. 4b, representative example, which produced errors of less than 6%).

As shown in Figs. 2 and 4b, satisfactory fittings were achieved to the experimental complex plane plots by using CPE in the equivalent circuit in place of C_{dl}, which has been used previously to model the mild steel/acid interface [29–32].

Table 1 C_{dl} values determined from Nyquist plots and Bode plots with their % deviation from fitting results

C_i(mM)	C_{dl}($\times 10^6$ sΩ^{-1}cm^{-2})				
	Nyquist	% Deviation	Bode	% Deviation	Fitting
Blank	318.7	−3.2	264.8	14.2	308.7
0.1	260.1	4.2	236.0	13.1	271.5
0.5	179.0	7.3	151.3	21.6	193.1
1	96.0	0.4	76.8	20.3	96.4
5	64.1	16.2	58.5	23.5	76.5

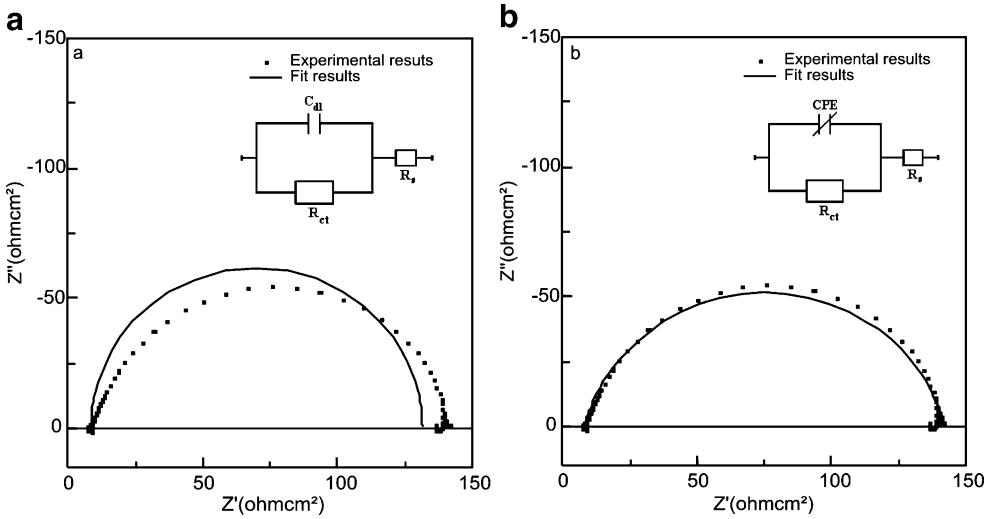

Fig. 4 Simulation of complex plane plot obtained in the presence of 0.1 mM Cys–Cys without (**a**) and with (**b**) taking into account the depression

The impedance of the CPE is given as [33]:

$$Z_{\mathrm{CPE}} = [Y_{\mathrm{o}}(j\omega)^{n}]^{-1}, \quad (2)$$

where Y_{o} is the magnitude of the CPE, j is the imaginary unit, ω is the angular frequency, and n is the phase shift gives details about the degree of surface inhomogeneity.

According to Eq. 2, Y_{o} is treated as C_{dl} only when n equals 1, i.e., when metal/solution interface behaves as an ideal capacitor. If not, use of Y_{o} as it was C_{dl} is just a simplification, which results poor quality of the fitting of the model to the experimental results (Fig. 4a).

In spite of the mentioned fact, the term, double layer capacitance, is still often used in the evaluation of AC impedance results to characterize the double layer believed to be formed at the metal/solution interface of systems displaying non-ideal capacitive behavior. For providing simple comparison between the capacitive behaviors of different corrosion systems, the values of Y_{o} were converted to C_{dl} as described elsewhere [34].

C_{dl} values determined from CPE parameters are also given in Table 1. Values determined by Eqs. 1a and 1b deviates from determined by fitting to some extent, but better results were obtained using complex plane plots.

Use of CPE in place of C_{dl} in the equivalent circuit model representing the metal/solution interface leads that the center of the capacitive loop rotates below the real axis up to a frequency independent constant phase angle, Fig. 2, [35]. The value of which can be used as a measure of deviation from an ideal capacitive behavior.

The AC impedance parameters extracted from the complex plane plots are given in Table 2. The R_{p} values were also measured at working electrode conditions using the common polarization resistance measurement technique and are given in the same table. The R_{p} values measured by common technique and obtained from complex plane plots (sum of the R_{s} and R_{ct}) are in good agreement with each other.

Table 2 shows that the addition of the Cys–Cys into the corrosive solution caused to an increase in the charge

Table 2 Impedance parameters extracted from complex plane plots in 0.5M H_2SO_4 solution in the absence and in the presence of various concentrations of Cys-Cys

Mol.	C_i(mM)	$-E_{\mathrm{corr}}$ (V)	R_{p} (Ω cm^2)[a]	R_{s} (Ω cm^2)[b]	R_{ct} (Ω cm^2)[b]	$\mathrm{CPE}_{\mathrm{dl}}$			C_{dl}($\times 10^6$ s Ω^{-1} cm^{-2})	IE%[d]
						Y_{o}($\times 10^6$ s^n Ω^{-1} cm^{-2})	n(0–1)	φ[c]		
Blank	–	0.530	58.0	8.3	51.1	566.3	0.848	13.7	308.7	–
Cys–Cys	0.1	0.518	145.4	7.9	134.7	460.6	0.831	15.2	271.5	62
	0.5	0.515	202.3	8.9	195.8	327.6	0.829	15.4	193.1	74
	1	0.516	277.6	8.2	249.5	149.2	0.879	10.9	96.4	80
	5	0.507	388.0	9.4	373.7	135.1	0.832	15.1	76.5	86

[a] R_{p} from polarization resistance measurements.
[b] R_{s} and R_{ct} from complex plane plots.
[c] Values of φ were calculated as described in ref. 35.
[d] Values of percent inhibition efficiency (IE %), were calculated using R_{ct} from complex plane plots.

transfer resistance and a decrease in the double layer capacitance given as [36]:

$$C_{dl} = \frac{\varepsilon_o \varepsilon}{d} S, \quad (3)$$

where ε_o is the vacuum dielectric constant, ε is the local dielectric constant, d is the thickness of the double layer, and S is the surface area of the electrode. According to Eq. 5, a decrease in C_{dl} can happen if the water molecules adsorbed on the mild steel surface replace with Cys–Cys molecules with lower dielectric constant. The capacitance is inversely proportional to the thickness of the double layer. Therefore, larger Cys–Cys molecules can decrease the C_{dl} by increasing the thickness of the double layer. The decrease in C_{dl}, which as mentioned caused by a decrease in local dielectric constant and/or an increase in the thickness of the electrical double layer [37–39], indicates the adsorption of Cys–Cys on the mild steel surface. In the absence and in the presence of Cys–Cys, phase shift value remains more or less identical, which indicates that the charge transfer process controls the dissolution mechanism [40] of mild steel in 0.5 M H_2SO_4 solution in the absence and in the presence of Cys–Cys. The values of φ are not ′0′ (in the range of 10.9 and 15.4) for both in the absence and in the presence of Cys–Cys as expected from the theory of AC impedance spectroscopy show that the metal/solution interface did not behave like an ideal capacitor.

Surface photographs were taken by means of scanning electron microscope (SEM) so as to determine if the inhibition is due to the formation of the film on the metal surface through adsorption (Fig. 5).

As can be seen from Fig. 5a, the electrode surface is strongly damaged in the absence of Cys–Cys. On the other hand, Fig. 5b shows that the surface heterogeneity decreased after the addition of Cys–Cys, providing considerable protection to mild steel against corrosion.

This observation is clearly proved by atomic force microscope (AFM) photographs taken in the range 0 to 2 μm at 25 °C after immersion in different test solutions. Three dimensional AFM photographs of mild steel electrodes in 0.5 M H_2SO_4 are shown in Fig. 6. A rough surface observed in the absence of Cys–Cys changes to a more smooth one in the presence of 5 mM Cys–Cys.

AC impedance results and surface morphology studies showed that the change in C_{dl} values was caused by the displacement of water molecules by the adsorption of Cys–Cys molecules on the mild steel surface. The adsorption is influenced from the molecule's chemical structure, the solution's chemical composition, the nature of the metal surface, the temperature, and the electrochemical potential at the metal/solution interface [41].

Besides their molecular form, amino acids can also be found as protonated species in acid solutions. Amino acid protonation is caused by the attachment of a proton to the nitrogen (N) atom of the NH_2 group [17]. Both molecular and protonated species can adsorb on the metal surface. However, adsorption of Cys–Cys by positively charged nitrogen atom cannot happen, as the steel surface is positively charged in acid solutions [42]. In that case, the high degree of percent inhibition efficiency must result from the adsorption of this compound at anodic sites of the mild steel surface with its molecular form. This view is strengthened with the polarization curves, whereby conspicuous effect of Cys–Cys on the anodic partial process can be seen, Fig. 7. Small decreases of cathodic current values may be caused by the adsorption of Cys–Cys by positively charged nitrogen atom on the positively charged metal surface through a charged intermediate, i.e., SO_4^{2-} anion adsorbed on the metal surface.

Assuming that organic molecules larger than water interact with each other in the adsorption layer, then the percent inhibition efficiency can be compared to fractional

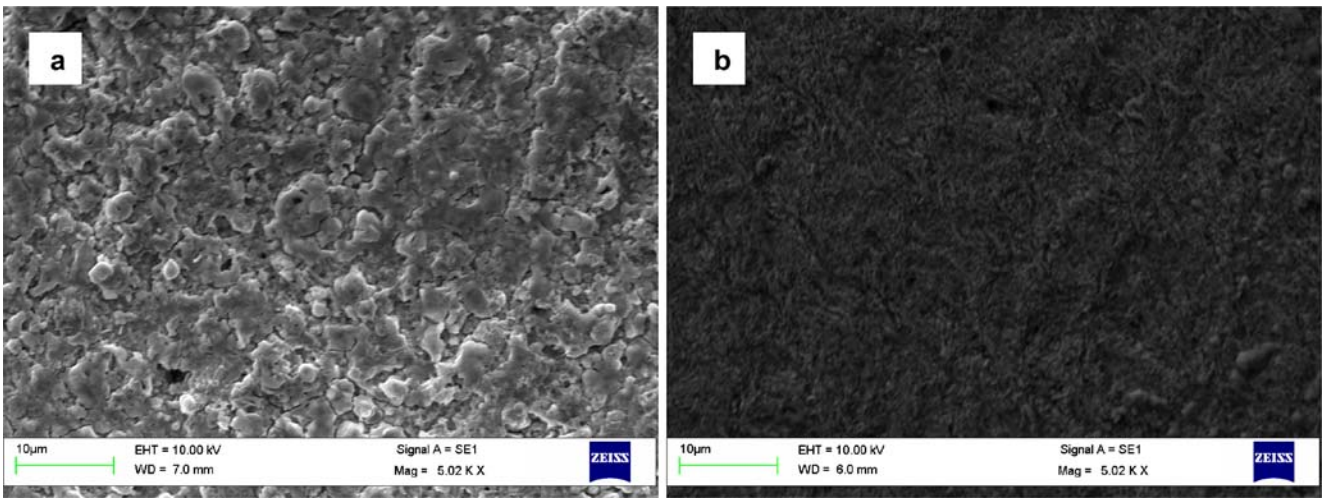

Fig. 5 SEM photographs of mild steel samples after immersion in 0.5 M H_2SO_4, in the absence (**a**) and in the presence of 5 mM Cys–Cys (**b**)

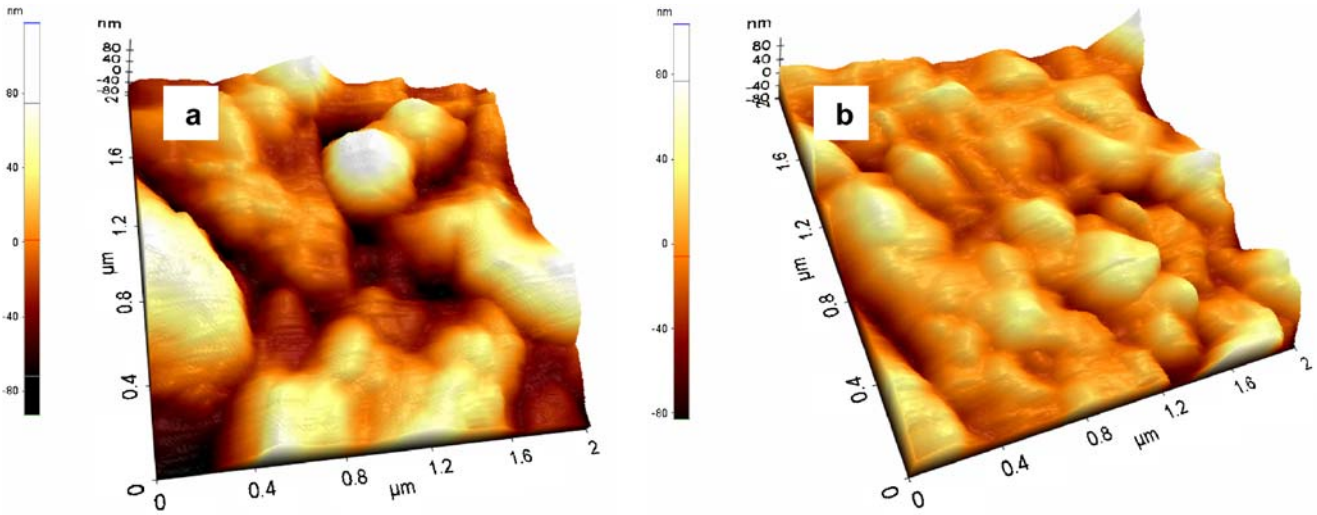

Fig. 6 AFM photographs of mild steel samples after immersion in 0.5 M H_2SO_4, in the absence (**a**) and in the presence of 5 mM Cys–Cys (**b**)

surface coverage, θ [43]. The values of θ were calculated using the following equation:

$$\theta = \frac{R_{ct}^{-1} - R_{ct(inh)}^{-1}}{R_{ct}^{-1}}, \quad (4)$$

where R_{ct} and $R_{ct(inh)}$ are the charge transfer resistance values in the absence and in the presence of Cys–Cys, respectively.

The adsorption isotherm in this study was not derived by direct measurements. Evaluation of the adsorption isotherm by way of AC impedance study is more convenient as the effect of the applied 5 mV rms sinusoidal perturbation onto the surface structure is not as large as to affect the results [44].

Among the most frequently used adsorption isotherm the Langmuir adsorption isotherm exhibited the best fit to the experimental data (Fig. 8).

Figure 8 shows that the slope of the Langmuir adsorption isotherm plot deviates from unity this behavior was attributed to the interactions between adsorbed inhibitor molecules on metal surface [18].

The Langmuir adsorption isotherm can be expressed as [45]:

$$\theta = \frac{KC}{1 + KC}, \quad (5)$$

where θ is the fractional coverage of the metal surface, C is the inhibitor concentration in the electrolyte, and K is the equilibrium constant for the adsorption/desorption process

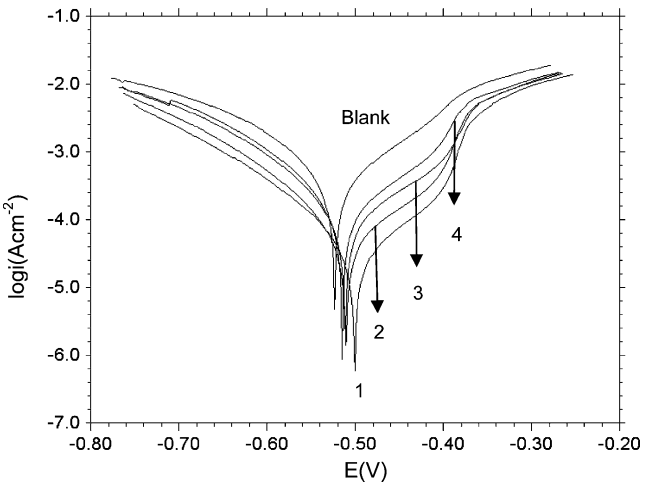

Fig. 7 Cathodic and anodic polarization curves for mild steel in 0.5M H_2SO_4 solution in the absence and in the presence of various concentrations of Cys–Cys. (1)5 mM, (2)1 mM, (3)0.5 mM and (4) 0.1 mM

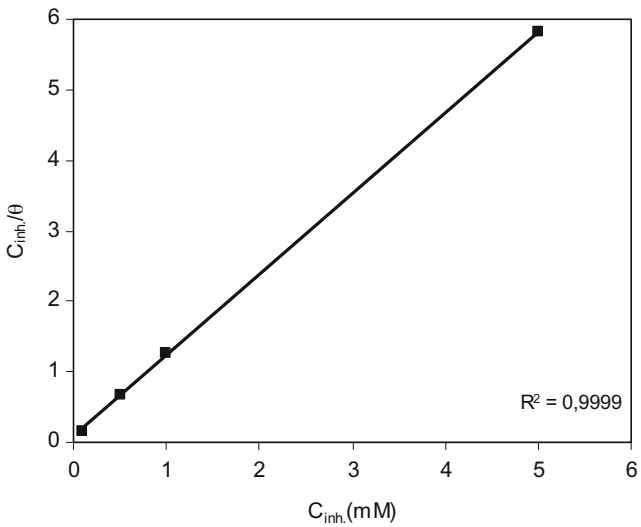

Fig. 8 Langmuir adsorption isotherm plot for mild steel in 0.5 M H_2SO_4 solution in the presence of various concentrations of Cys–Cys

Table 3 The energies of frontier orbitals for Cys–Cys, iron and energy gaps for the interaction

Parameters	Cys–Cys	Iron[a]
E_{HOMO}(eV)	−6.670	−7.81
E_{LUMO}(eV)	−1.196	−0.25
ΔE^{b}	6.614	–
ΔE^{c}	6.420	–

[a] HOMO and LUMO values for iron were taken as ionization potential and electron affinity, respectively [50].
[b] $LUMO_{Cyst.}$–$HOMO_{Fe}$
[c] $LUMO_{Fe}$–$HOMO_{Cyst}$

and it is related to the standard free energy of adsorption $\left(\Delta G^{\circ}_{ads}\right)$ according to the following equation [46]:

$$K = \frac{1}{55.5}\exp\left(\frac{-\Delta G^{o}_{ads}}{RT}\right), \quad (6)$$

where R is the universal gas constant and T is the absolute temperature. The value of ΔG°_{ads} was found as −33.2 kJ/mol. The high negative value of ΔG°_{ads} of Cys–Cys indicates that this compound is strongly adsorbed on the mild steel surface. In general, values of ΔG°_{ads} by −20 kJ/mol are compatible with the electrostatic interaction between the charged molecules and the charged metal. Those which are more negative than −40 kJ/mol entail charge sharing or charge transfer from the inhibitor molecules to the metal surface [41]. The calculated ΔG°_{ads} value, being closer to −40 kJ/mol, is between the threshold values for physical adsorption and chemical adsorption indicates that adsorption of Cys–Cys on mild steel surface involves two types of interaction.

Theoretical study

The adsorption of neutral organic molecules on the metal surface, which entails charge sharing or charge transfer between organic molecules and the metal surface, is achieved by an appropriate overlap of frontier orbitals, i.e., the highest occupied molecular orbital (HOMO) and the lowest unoccupied molecular orbital (LUMO) [47, 48]. While this adsorption happening, one of the reacting species acts as an electron pair donor and another one acts as an electron pair acceptor. Therefore, energies of the frontier orbitals should be taken into account. Energy level of LUMO represents the ability of the molecule to receive charge when interacting with electron pair donors; on the other hand, the energy level of HOMO represents its ability to donate charge when interacting with electron seeking reagents. As the energy gaps among the frontier orbitals decrease, interactions between the reacting species become stronger [49]. Energies of the frontier orbitals for Cys–Cys and iron, and energy gaps for the interactions are given in Table 3.

The energy gap between the HOMO of the metal atom and the LUMO of the Cys–Cys molecule is close to the one between the HOMO of the Cys–Cys molecule and the LUMO of the metal atom. This finding indicates that the Cys–Cys molecules can act as both electron pair donors and electron pair acceptors while adsorbing on the mild steel surface.

Since, in the ground state, the frontier orbitals take part in the activity properties of corrosion inhibitors, their HOMO and LUMO densities are important for the charge transfer. As for the frontier molecular orbital coefficients, the HOMO and the LUMO densities were plotted as given in Fig. 9.

As can be seen from Fig. 9, Cys–Cys displays an effect of retrodonation, which is due to the fact that the molecular orbital coefficients for both the HOMO and the LUMO are rather high for the same centers [51]. This enables us to confirm the experimentally obtained results for the inhibition action of Cys–Cys, since, considering the theory; that introducing a good inhibitor should be either a good electron donor or a good electron acceptor so as to stabilize the electron deficiency or electron abundance on active metal sites that are liable to corrosion [52].

Conclusions

– AC impedance spectroscopy, polarization resistance measurement, and polarization curves measurement results indicated that Cys–Cys is a good and effective inhibitor for mild steel corrosion in 0.5 M H_2SO_4. The percent inhibition efficiency changes with concentration (the highest percent inhibition efficiency in results was 86).

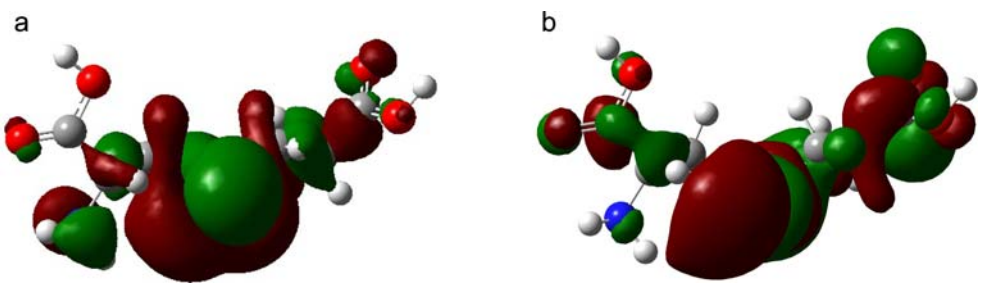

Fig. 9 **a**. Highest occupied molecular orbital (HOMO); **b**. Lowest unoccupied molecular orbital (LUMO) surfaces for Cys–Cys molecule

- The nonideal capacitive behavior of the mild steel/sulfuric acid interface was taken into account by placing a constant phase element (CPE) in the equivalent circuit model, which significantly improved the quality of fitting process.
- The SEM and AFM photographs showed that the inhibition is due to the formation of the film on the metal surface through adsorption of Cys–Cys molecules.
- Langmuir adsorption isotherm exhibited the best fit to the experimental data with a standard free energy of adsorption, ΔG°_{ads}, of −33.2 kJ/mol, which indicates that Cys–Cys molecules strongly adsorb on the mild steel surface.
- Energy gaps for the interactions between mild steel surface and Cys–Cys molecule were found to be close to each other, showing that Cys–Cys owns the capacity to behave as both electron donor and electron acceptor.
- Distribution of the frontier molecular orbitals on the Cys–Cys molecule specified that it has an effect of retrodonation as molecular orbital coefficients for both the HOMO and the LUMO are rather high for the same centers.

Acknowledgment The experimental studies of this work were carried out at Physical Chemistry Research Laboratory of Chemistry Department, Çukurova University.

The author would like to thank Professor Dr İlyas Dehri (Department of Chemistry, Cukurova University) and Assistant Professor Dr Faruk Karadağ (Department of Physics, Cukurova University) for their discussions and comments.

The author is also grateful to Associate Professor Dr Mustafa Çulha (Department of Genetics and Bioengineering, Yeditepe University) for SEM and AFM photographs.

References

1. Mccafferty E (1997) Corros Sci 39:243
2. Lagrenée M, Mernari B, Bouanis M, Traisnel M, Bentiss F (2002) Corros Sci 44:573
3. Quraishi MA, Rawat J (2003) Mater Chem Phys 77:43
4. Özcan M, Dehri İ, Erbil M (2004) Appl Surf Sci 236:155
5. Wang H, Liu R, Xin J (2004) Corros Sci 46:2455
6. Migahed MA (2005) Mater Chem Phys 93:48
7. Ashassi-Sorkhabi H, Shaabani B, Seifzadeh D (2005) Electrochim Acta 50:3446
8. Jeyaprabha C, Sathiyanarayanan S, Venkatachari G (2005) Appl Surf Sci 246:108
9. Chetouani A, Daoudi M, Hammouti B, Ben Hadda T, Benkaddour M (2006) Corros Sci 48:2987
10. Bentiss F, Gassama F, Barbry D, Gengembre L, Vezin H, Lagrenée M, Traisnel M (2006) Appl Surf Sci 252:2684
11. Khaled KF (2006) Appl Surf Sci 252:4120
12. Dehri İ, Özcan M (2006) Mater Chem Phys 98:316
13. Bentiss F, Bouanis M, Mernari B, Traisnel M, Vezin H, Lagrenée M (2007) Appl Surf Sci 253:3696
14. Benali O, Larabi L, Traisnel M, Gengembre L, Harek Y (2007) Appl Surf Sci 253:6130
15. Walter GW (1986) Corros Sci 26:681
16. Dehri İ, Erbil M (1999) Br Corros J 34:299
17. Abiola OK (2005) J Chilean Chem Soc 50:685
18. Oguzie EE, Li Y, Wang FH (2007) Electrchim Acta 53:909
19. Oguzie EE, Li Y, Wang FH (2007) J Colloid Interface Sci 310:90
20. Oguzie EE, Li Y, Wang FH (2007) Electrochim Acta 52:6988
21. Abd-El-Nabey BA, Khalil N, Mohamed A (1985) Surf Technol 24:383
22. Lee C, Yang W, Parr RG (1988) Phys Rev B 37:785
23. Becke AD (1993) J Chem Phys 98:5648
24. Frisch MJ, Trucks GW, Schlegel HB, Scuseria GE, Robb MA, Cheeseman JR, Montgomery JA Jr, Vreven T, Kudin KN, Burant JC, Millam JM, Iyengar SS, Tomasi J, Barone V, Mennucci B, Cossi M, Scalmani G, Rega N, Petersson GA, Nakatsuji H, Hada M, Ehara M, Toyota K, Fukuda R, Hasegawa J, Ishida M, Nakajima T, Honda Y, Kitao O, Nakai H, Klene M, Li X, Knox JE, Hratchian HP, Cross JB, Adamo C, Jaramillo J, Gomperts R, Stratmann RE, Yazyev O, Austin AJ, Cammi R, Pomelli C, Ochterski JW, Ayala PY, Morokuma K, Voth GA, Salvador P, Dannenberg JJ, Zakrzewski VG, Dapprich S, Daniels AD, Strain MC, Farkas O, Malick DK, Rabuck AD, Raghavachari K, Foresman JB, Ortiz JV, Cui Q, Baboul AG, Clifford S, Cioslowski J, Stefanov BB, Liu G, Liashenko A, Piskorz P, Komaromi I, Martin RL, Fox DJ, Keith T, Al-Laham MA, Peng CY, Nanayakkara A, Challacombe M, Gill PMW, Johnson B, Chen W, Wong MW, Gonzalez C, Pople JA (2003) Gaussian 03, Revision B.03. Gaussian, Inc., Pittsburgh, PA
25. Gauss View (2003) Version 3.0. Gaussian, Pittsburgh PA
26. Juttner K (1990) Electrochim Acta 35:1501
27. Morad MS (2000) Corros Sci 42:1307
28. Kelly RG, Scully JR, Shoesmith DW, Buchheit RG (2003) Electrochemical techniques in corrosion science and engineering. Marcel Dekker, New York
29. Popova A, Raicheva S, Sokolova E, Christov M (1996) Langmuir 12:2083
30. Popova A, Sokolova E, Raicheva S, Christov M (2003) Corros Sci 45:33
31. Popova A, Christov M (2006) Corros Sci 48:3208
32. Popova A (2007) Corros Sci 49:2144
33. Ma H, Cheng X, Li G, Chen S, Quan Z, Zhao S, Niu L (2000) Corros Sci 42:1669
34. Hosseini M, Mertens SFL, Ghorbani M, Arshadi MR (2003) Mater Chem Phys 78:800
35. Martinez S, Metikoš-Huković M (2003) J Appl Electrochem 33:1137
36. Bentiss F, Lagrenée M, Elmehdi B, Mernari B, Traisnel M (2002) Corrosion 58:399
37. McCafferty E, Hackerman N (1972) J Electrochem Soc 119:146
38. Babić-Samardžija K, Lupu C, Hackerman N, Barron AR, Luttge A (2005) Langmuir 21:12187
39. Babić-Samardžija K, Khaled KF, Hackerman N (2005) Anti-Corros Methods Mater 52:11
40. Hermas AA, Morad MS, Wahdan MH (2004) J Appl Electrochem 34:95
41. Moretti G, Quartarone G, Tassan A, Zlngales A (1996) Electrochim Acta 41:1971
42. Trasatti S (1971) J Electroanal Chem 33:351
43. Hosseini MG, Ehteshamzadeh M, Shahrabi T (2007) Electrochim Acta 52:3680
44. Lebrini M, Lagrenée M, Vezin H, Traisnel M, Bentiss F (2007) Corros Sci 49:2254
45. Agrawal R, Namboodhiri TKG (1990) Corros Sci 30:37

46. Ateya BG, El Anadoli BE, El-Nizamy FM (1984) Corros Sci 24:509
47. Bentiss F, Traisnel M, Lagrenée M (2001) J Appl Electrochem 31:41
48. Martinez S (2003) Mat Chem Phys 77:97
49. Huang W, Tan Y, Chen B, Dong J, Wang X (2003) Tribol Int 36:163
50. Mutombo P, Hackerman N (1998) Anti-Corros Methods Mater 45:413
51. Gómez B, Likhanova NV, Domínguez-Aguilar MA, Olivares O, Hallen JM, Martínez-Magadan JM (2005) J Phys Chem A 109:8950
52. Höpfl H, Gómez B, Palou RM (2005) J Mex Chem Soc 49:307